Effect of protein adsorption on cell uptake and blood clearance of methoxy poly(ethylene glycol)-poly(caprolactone) nanoparticles

Jing Li,[1][*] Ninghua Wu,[1][*] Jiliang Wu,[1] Ying Wan,[2] Chao Liu[1]

[1]Hubei Province Key Laboratory on Cardiovascular, Cerebrovascular, and Metabolic Disorders, Hubei University of Science and Technology, Xianning, Hubei 437100, People's Republic of China
[2]College of Life Science and Technology, Huazhong University of Science and Technology, Wuhan 430074, People's Republic of China
*These authors contributed equally to this work.
Correspondence to: Y. Wan (E-mail: ying_wan@hust.edu.cn) and C. Liu (E-mail: xn_liuchao@163.com)

ABSTRACT: The interactions between nanoparticles and cells or tissues are frequently mediated by different biomolecules adsorbed onto the surface of nanoparticles. In this study, several methoxy poly(ethylene glycol)-poly(ε-caprolactone) (mPEG-PCL) copolymers with various mPEG/PCL ratios were synthesized and used to produce three types of mPEG-PCL nanoparticles. The protein-adsorption behavior of nanoparticles was assessed using fetal-bovine-serum (FBS) as a model protein. The cell uptake of nanoparticles at different nanoparticle doses as well as various culture periods was examined by measuring their endocytosis rate related to Hela cells cultured in FBS-free and FBS-contained media. The blood clearance of nanoparticles was evaluated using Kunming mice to see the differences in circulation durations of nanoparticles. Results suggest that that FBS is able to significantly regulate the cell uptake of nanoparticles *in vitro*, and on the other hand, the size and mPEG/PCL molar ratio of mPEG/PCL nanoparticles are closely correlated to their blood clearance. © 2015 Wiley Periodicals, Inc. J. Appl. Polym. Sci. **2016**, *133*, 42884.

INTRODUCTION

Chemotherapy has commonly been used alone or combinatorially with surgical intervention or radiotherapy for a variety of cancers.[1–4] The clinical outcomes of chemotherapy are considered to be closely associated with the properties of chemotherapeutic agents themselves and the administration of agents besides some other factors. Despite many successful cases, chemotherapy for cancers is frequently limited because many chemotherapeutic agents have poor aqueous solubility, instability in blood, and non-selectivity, which results in low bioavailability and various degrees of toxicity to normal tissues.[5] To reduce side effects or toxicity of chemotherapeutic agents and increase their therapeutic efficacy, different nanoscale vehicles for chemotherapeutic agents, such as nanoparticles, nanogels, and nanocapsules, have been largely developed by using various materials and techniques.[6]

In point of nano carriers for delivery of poor water-soluble drugs, biocompatible and biodegradable polymers have attracted much attention due to their tailorable structures and properties as well as processability in favor of various carrier forms. Of different polymers, methoxy poly(ethylene glycol)-poly(ε-caprolactone) (mPEG-PCL) has been widely used as carriers and it can be self-assembled into polymeric nanoparticles due to its hydrophobic PCL and hydrophilic mPEG segments.[7,8] By changing the segment ratios, mPEG-b-PCL nanoparticles with various sizes can be endowed with abilities to load different hydrophobic drugs with high efficacy, enhance the stability of drugs, facilitate the sustained drug release, and extend the half-time of drugs *in vivo*.[8–10]

It is know that nanoparticles (NPs) are usually opsonified by different proteins once they are exposed to a physiological environment *in vivo*, and as a result, a layer of proteins, commonly being named as protein corona, will immediately form on the surface of NPs when NPs enter the blood vessel.[11] In general, the protein corona would alter the size, aggregation state, and surface properties of nanoparticles, and thus, enable the NPs to have an additionally biological identity differed from its original physicochemical identity. It is clear that the biological identity of NPs can mediate the interactions between NPs and biomolecules, resulting in quite different physiological responses.[12] Unfortunately, many opsonins, such as immunoglobulins, fibrinogen, and complement proteins, promote the phagocytosis and rapid clearance of the NPs from the bloodstream.

To date, several investigations for the cell uptake involved in various NPs and different cells have pointed out that the uptake levels considerably depend on whether nanoparticles are exposed to fetal-bovine-serum (FBS)-free medium or FBS-contained medium.[13–19] Nevertheless, details on the uptake in these studies still need to be clearified.[20,21]

It has been observed that in most cases, cell uptake of NPs under serum-free conditions is higher than that measured for the same NPs in the presence of serum[13–17] or in a more simple protein solution.[19] In addition, more studies have confirmed that properties of NPs themselves are also affected by the presence or absence of a protein coating (or other coatings) on their surface, and in certain cases, the presence of protein corona on the surface of NPs can mitigate the toxicity of bare NPs to some extent.[22–26]

It is generally difficult to figure out the detailed mechanisms for protein adsorption on the surface of NPs and the related properties of protein-adsorbed NPs due to complicated interactions among the proteins and NPs. Nevertheless, electrostatic and hydrophobic interactions have been used to explain the adsorption modes of protein based on a fact that hydrophobic NPs tend to occur stronger interactions with proteins than hydrophilic ones.[27]

Despite many studies on mPEG-b-PCL NPs, to our knowledge, there are limited data available for their protein adsorption behaviors and the effect of protein corona on their cell uptake and blood clearance *in vivo*. In the present study, an attempt was thus made to examine the interactions between mPEG-PCL NPs and FBS using a fluorescent tracing method. FBS medium was chosen as a model protein solution in consideration of its similarity to the human blood plasma and its known properties. It is expected that the results presented in this study could not only provide cues for the design of mPEG-PCL based nano-drugs but also for the half-life extension of other nanoparticles *in vivo*.

MATERIALS AND METHODS

Materials

Rhodamine B (RhB), 4,6-diamidino-2-phenylindole (DAPI), 4-dimethylaminopyrridine (DMAP), *N*-acetyl-L-cysteine (NAC), *N*,*N*'-dicyclohexylcarbodiimide (DCC), ε–caprolactone (CL), 3-(4,5-dimethylthiazol-2-yl)-2,5-diphenyl tetrazolium bromide (MTT), methoxy poly(ethylene glycol) (mPEG, $M_n = 5000$), and stannous octoate (Sn(Oct)$_2$) were purchased from Sigma-Aldrich. Dulbecco's Modified Eagle's Medium (DMEM) was received from Gibco. Methanol and acetic acid (HPLC grade) were purchased from Fisher Scientific. Dimethyl sulfoxide (DMSO) and acetone were purchased from Liaoning Kelong Fine Chemical Co. (China). mPEG samples were dried by azeotropic distillation using toluene, and then, were further vacuum-dried at 50°C for 12 h before use. CL was purified by drying over CaH$_2$ at room temperature and distilling under reduced pressure. Other chemicals were obtained from different commercial sources in china and used without further purification.

Measurements

^{1}H-NMR spectra were measured by a Unity 300-MHz NMR spectrometer (Bruker, Germany) at room temperature. The morphology of the nanoparticles was viewed using a JEOL JEM-1011 transmission electron microscope (TEM). Colloidal nanoparticle suspensions were prepared using ultrapure water and they were evaluated by dynamic light scattering (DLS) measurements using an instrument (DAWN EOS, Wyatt Technology) to determine hydrodynamic particle sizes. The zeta potential (ζ) of nanoparticles was also measured on the same instrument.

Synthesis of mPEG-PCL

The mPEG-PCL was synthesized following a ring-opening polymerization method described elsewhere.[28] In a typical procedure, 17 g of CL, 15 g of mPEG, and 0.16 g of Sn(Oct)$_2$ were introduced into the reactor under a dry nitrogen atmosphere, and the reaction was allowed to conduct at 130°C for 6 h. The reaction was stopped by cooling the reaction system to the room temperature. The resultant copolymer was separated by precipitating in diethyl ether, followed by drying in vacuum at 25°C. By mainly changing the feed ratio of CL to mPEG and the reaction time, three types of mPEG-PCLs with varied mPEG/PCL molar ratios at around 5/2, 5/3, and 5/4 were synthesized. The purified copolymers were kept in desiccators for further use.

Synthesis of Rhodamine B-Labeled mPEG-PCL

RhB was labeled onto the mPEG-PCL copolymers via a regular coupling reaction using DCC and DMAP as active reagents. About 0.5 g of mPEG-PCL and 0.001 g of RhB were dissolved in 10 mL of methylene chloride, followed by the addition of 0.17 g of DCC and 0.05 g of DMAP, respectively. The mixture was kept stirring in an ice bath shielding from light for 24 h, and was then precipitated with excess diethyl ether. After being filtered, the RhB-labeled mPEG-PCL copolymer was vacuum-dried. The product was further purified by dialyzing again water and freeze-dried again. Three types of mPEG-PCLs were labeled with RhB using the same method.

Preparation of Nanoparticles

The presently synthesized mPEG-PCLs can be self-assembled into nanoparticles in aqueous media due to their amphiphilic properties. A reported method was employed for the preparation of mPEG-PCL nanoparticles.[29] Briefly, 10 mg of RhB-labeled mPEG-PCL was dissolved in 3 mL tetrahydrofuran (THF) in a round bottom flask and the THF was then evaporated using rotary evaporation at 50°C to obtain a solid film. The resulting film was further hydrated using 10 mL water at 50°C for 30 min to produce a nanoparticle solution. The solution was dialyzed against distilled water for 24 h, followed by lyophilization to obtain RhB-labeled mPEG-PCL nanoparticles. The preparation was performed by shielding from light. Three types of RhB-labeled mPEG-PCL nanoparticles with molar ratio of mPEG to PCL at around 5/2, 5/3, and 5/4 were named as NP2K, NP3K, and NP4K, respectively.

Cell Culture

Human cervix cancer Hela cell line was provided by the cell bank of the Shanghai Institutes for Biological Sciences. Hela cells were expanded in DMEM at 37°C in a humidified 5% CO$_2$ atmosphere, supplementing with 10% FBS, 100 U/mL penicillin, and 100 mg/mL streptomycin. Cultured medium was replaced on alternate days until confluence, and the harvested cells were resuspended in media for further experiments.

Cytotoxicity Assay

Hela cells harvested at the logarithmic growth phase were seeded in 96-well plate at a cell density of 1×10^5 cells/well and incubated with DMEM at 37°C for 24 h. The medium was then replaced with nanoparticles solutions in DMEM at different equivalent concentrations changing from 0.32 μg/mL to 1.0 mg/mL. After incubation for additional 48 h, each well was added with 20 μL of MTT solution (5 mg/mL) in PBS, and the plate was further incubated at 37°C for 4 h, followed by removal of culture medium and addition of 150 μL DMSO to dissolve the formazan crystals formed. Finally, the plate was shaken for 10 min, and the absorbance of formazan products was measured at 570 nm using a microplate reader. Cell viability was determined with reference to two-dimensional culture without nanoparticle treatment.

Protein Adsorption on Nanoparticles

About 0.5 mL of nanoparticle dispersion solutions with different concentrations (0.5 mg/mL, 1 mg/mL, 2 mg/mL, and 4 mg/mL) was added into 0.5 mL of deionized water or 20% FBS, and incubated under agitation for 2 h in eppendorf tubes at 37°C, followed by centrifugation at 3000 rpm for 5 min. The soluble protein left in the culture medium after incubation was separated by ultrafiltration at 3000 rpm for 5 min, and analyzed using a bicinchoninic acid (BCA) essay. Deionized water was used as control and its optical density value was deducted from measured values matched with respective nanoparticle samples.

Cell Uptake

Hela cells were seeded in 6-well culture plates with complete DMEM medium containing 10% FBS at a density of 5×10^4 cells per well and allowed to adhere for 24 h. After that, the culture medium was removed, and cells were washed with PBS prior to the treatment of nanoparticle dispersion solutions.

The RhB-labeled mPEG-PCL nanoparticle stock solution (4 mg/mL) was diluted into several less concentrated solutions with prescribed concentrations using FBS-free or FBS-contained DMEM medium (10% FBS), and to each well (5×10^4 cells), a given amount of the diluted mPEG-PCL solution was added. After co-culture with nanoparticles for 60 min, the culture medium containing RhB-labeled mPEG-PCL nanoparticles was vacuated and the cells were washed three times with PBS. Cells were then harvested using trypsin/Ethylene Diamine Tetraacetic Acid and fixed with a 4% formalin solution for 20 min. After that, the cells were resuspended in PBS for subsequent flow cytometry measurements. Average endocytosis rate was determined by counting a minimum of 10,000 cells for each specimen. To quantitatively compare the effect of FBS-adsorption on the cell uptake of nanoparticles, after culture for 60 min, the nanoparticle concentration matched with the endocytosis rate at 50% (EC_{50}) was measured in both FBS-free and FBS-contained media based on the fitted curves of endocytosis rate versus nanoparticle concentration.

For confocal imaging, Hela cells were seeded into 6-well culture dishes in which each well was placed with a glass cover-slip with a diameter of 15 mm, and the cell density was set as 2×10^4 cells per well. After 24-h adherence, the cells were treated with RhB-labeled mPEG-PCL nanoparticles using the same method described above for the sample preparation in flow cytometry measurements. After removal of the culture medium containing RhB-labeled mPEG-PCL nanoparticles, the cells were washed with PBS, fixed with 4% formaldehyde (1 mL/well) at room temperature for 10 min, followed with washing using PBS. For nucleus staining, the fixed cells in each well were incubated with 1 mL of DAPI solution (1.0 g/mL) for 10 min, and washed with PBS five times. The cover-slips were then taken out for confocal laser scanning microscopy analysis.

Blood Clearance

All animal experiments were conducted according to National Institutes of Health standards as set forth in the guide for the care and use of laboratory animals. Twenty-seven Kunming mice (6–8 weeks) were randomly divided into nine groups. The mice were injected with RhB labelled mPEG-PCL nanoparticles via the tail vein at an equivalent dose of 50 mg/kg of body weight. Blood samples were collected via the eye socket using heparinized tubes at predetermined time intervals at 10 min, 60 min, and 4 h after injection. The blood samples were centrifuged at 3000 rpm for around 10 min, and the supernatants were used for fluorescent analysis. The fluorescence intensities of supernatants were measured using a fluorescence spectrometer (Nikon Instruments Europe B.V., Surrey, England) at an excitation wavelength of 558 nm and an emission wavelength of 590 nm.

Statistical Analysis

Data were expressed as means $\pm$ standard deviation (n$\geq$3). Statistical analyses were carried out using statistical software (GraphPad Prism). One-way ANOVA was used to examine whether significant differences existed between the measured data, and $P<0.05$ was considered to be statistically significant.

RESULTS AND DISCUSSION

Parameters of mPEG-PCL Nanoparticles

Several mPEG-PCL copolymers were first synthesized in order to prepare mPEG-PCL nanoparticles having different average sizes and properties. By mainly changing the feed ratio of CL to mPEG and the reaction time while keeping other reaction condition constant, it was found that the segment of PCL in mPEG-PCLs could be well controlled. Based on many trials, the molar ratios of mPEG to PCL was optimized as around 5/2, 5/3, and 5/4, and the resulting mPEG-PCLs were further used to produce RhB-labeled mPEG-PCL copolymers for preparing three types of nanoparticles, named as NP2K, NP3K, and NP4K, respectively. Figure 1 presents three representative TEM images for these nanoparticles. It can be reached that these nanoparticles showed basic sphericity without aggregation and their size was estimated to be several tens of nanometers. Figure 2 shows several representative size-distributions for three types of nanoparticles. The curves indicated that these size-distributions had approximate Gaussian-distribution characters, and the peak values matching with the size for NP2K, NP3K, and NP4K nanoparticles were about 60, 120, and 150 nm, respectively. Three sets of nanoparticle samples were measured for their average size and zeta potential, and relevant data are listed in Table I. It can be seen that these nanoparticles had significantly different ($P<0.01$) average sizes but similar zeta potentials. In the present study, the M_n of used mPEG was
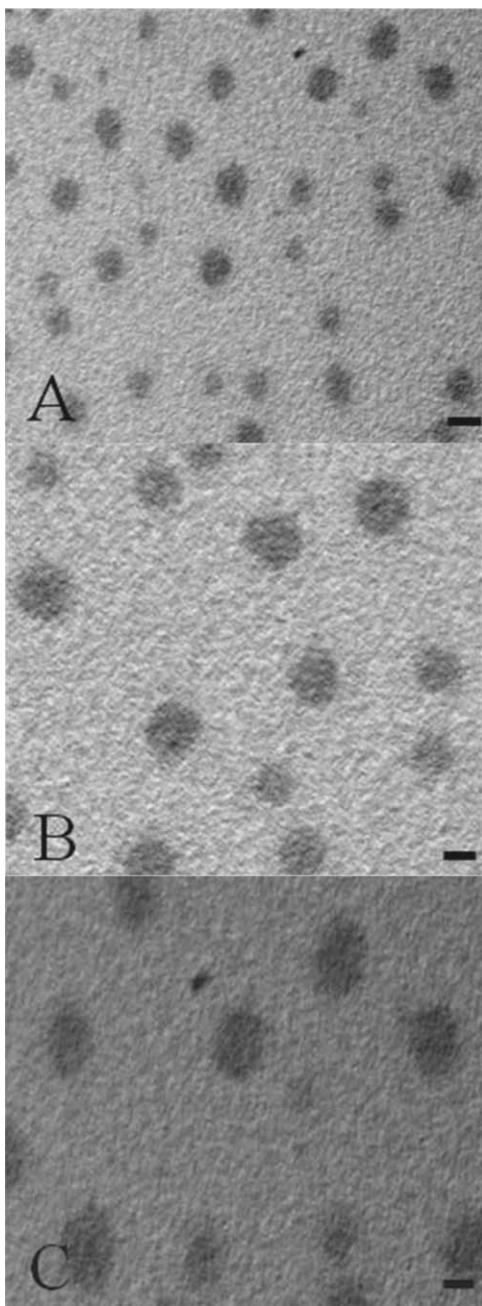
Figure 1. TEM images of NP2K (A), NP3K (B), and NP4K (C) nanoparticles (scale bar: 100 μm).

Figure 2. Representative size-distributions measured by DLS for NP2K, NP3K, and NP4K nanoparticles. [Color figure can be viewed in the online issue, which is available at wileyonlinelibrary.com.]

the nanoparticles since these nanoparticles were prepared in aqueous media. In addition, NP2K, NP3K, and NP4K nanoparticles had different average sizes. The various lengths of hydrophobic PCL segments in mPEG-PCLs and different sizes of mPEG-PCL nanoparticles may synergetically regulate the surface properties of mPEG-PCL nanoparticles, resulting in insignificant differences in the zeta potential of nanoparticles.

Viability of Hela Cells Cultured with Nanoparticles

To see whether presently prepared nanoparticles have any cytotoxicity to Hela cells, three types of nanoparticles were respectively cultured with Hela cells at various doses of nanoparticles for 48 h and the viability of Hela cells was assessed using a MTT essay. Figure 3 shows changes in the viability of Hela cells cultured with different nanoparticles as the nanoparticle concentration increased from 0.32 μg/mL to 1.0 mg/mL. It can be observed that within the overall tested range of nanoparticle concentration, the viability of Hela cells was higher than 90%, suggesting that NP2K, NP3K, and NP4K nanoparticles are nearly nontoxic to Hela cells.

Protein Adsorption of Nanoparticles

In general, the effect of *in vivo* opsonization on nanoparticles can lead to the rapid *in vivo* clearance of nanoparticles through the mononuclear phagocytic system, which is considered to be a major obstacle for delivery of drugs via nanoscale carriers. To date, it is basically clear that the opsonization process involves protein adsorption and/or activation. When nanoparticles are intravenously injected into body, they will interact with different biomolecules, such as proteins and lipids, to different extent, and these biomolecules will in turn influence the biodistribution and metabolism of nanoparticles.[30,31] In the present study, an effort was made to see the effect of FBS adsorption on cell uptake of mPEG-PCL nanoparticles. The amount of absorbed FBS was determined by the difference between the initial FBS amount and the FBS amount left in the supernatant after adsorption. Figure 4 shows the amount of adsorbed FBS on different nanoparticles. To each type of nanoparticles, an increasing FBS-adsorption trend was observed as the nanoparticle concentration increased. Considering the differences in the PCL segments

5000, and mPEG-PCLs used for NP2K, NP3K, and NP4K nanoparticles had gradually extended length of hydrophobic PCL segments due to the designated molar ratios of mPEG to PCL. As a result, NP2K nanoparticles should have smaller average sizes than two others because the mPEG-PCL used for the preparation of NP2K nanoparticles had shorter chain length than two others. The difference in average sizes between NP3K and NP4K nanoparticles was due to the same reason.

It is know that mPEG-PCLs had some amphiphilic features. The hydrophobic PCL segments could tend to aggregate inside the mPEG-PCL nanoparticles whilst the relatively hydrophilic PEG segments may be more likely to expose on the surface of
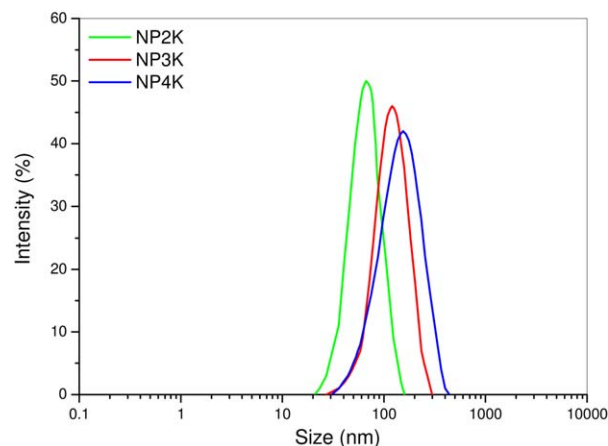
Table I. Main Parameters of RhB-Labeled mPEG-PCL Nanoparticles

Sample name	Estimated molar ratio of mPEG to PCL[a]	Mean size (nm)[b]	PDI	ζ(mV)
NP2K	5:2	67.7 ±5.17	0.11 ± 0.051	−8.1 ± 0.45
NP3K	5:3	120.6 ± 9.17	0.16 ± 0.039	−6.6 ± 0.37
NP4K	5:4	154.9 ± 11.25	0.23 ± 0.064	−7.2 ± 0.58

[a] The chemical composition and molar ratio of mPEG to PCL were determined using ^{1}H NMR spectra.
[b] Data were obtained by DLS measurements.

among these nanoparticles, it can also be deduced that the FBS-adsorbed amount increased with increasing length of PCL segments. To quantitatively determine the FBS adsorption, the concentration at 50% of maximal effect (EC_{50}) was measured. The EC_{50} for NP2K, NP3k, and NP4K was 4.0, 2.96, and 1.75 mg/ml, respectively.

These results indicated that nanoparticles built by the mPEG-PCL with shorter hydrophobic PCL segments, for example, NP2K nanoparticles, had better anti-opsonization ability than those prepared with the mPEG-PCL having longer hydrophobic PCL segments. In the case of liposomes, it has been reported that protein adsorption onto liposomes makes them more susceptible to phagocytosis, and protein adsorption usually becomes stronger on hydrophobic surface than on hydrophilic surfaces.[32] In our cases, NP4K nanoparticles had largest EC_{50}, implying the surface of NP4K nanoparticles may less hydrophilic than others.

Cell Uptake

To figure out the effect of FBS-adsorbed nanoparticle concentrations on the cell uptake, NP2K, NP3K, and NP4K nanoparticles were respectively incubated with Hela cells for 60 min using FBS-free or FBS-contained culture (10% FBS) media. The endocytosis rate of nanoparticles was determined using flow cytometry analysis and relevant data are depicted in Figure 5. It can be observed that (1) the endocytosis rates for three types of nanoparticles were concentration-dependent in both FBS-free and FBS-contained media; (2) much lower concentration of NP2K

nanoparticles was needed to reach the same endocytosis rate when comparing to NP3K or NP4K nanoparticles in both FBS-free and FBS-contained culture media; and (3) in the cases of NP3K and NP4K nanoparticles, higher endocytosis rates were recorded in FBS-free medium than in FBS-contained medium at the designated nanoparticle concentration range corresponding to each type of nanoparticles. These results suggest that the smaller mPEG-PCL nanoparticles will be more easily uptaken by Hela cells than those larger ones, and on the other hand, FBS-adsorption onto the mPEG-PCL nanoparticles would hinder their uptake by Hela cells. To see the effect of FBS-adsorption on the cell uptake of nanoparticles, EC_{50} was measured and the relevant data are listed in Table II. To each type of nanoparticles, ΔEC_{50} can be related to the single contribution arisen from FBS-adsorption. Data in Table II reveal that FBS-adsorption had nearly no impact on the uptake of NP2K nanoparticles, but it significantly regulated the uptake of NP3K and NP4K nanoparticles. In general, cellular uptake of nanoparticles could be affected by many factors, such as particle size,[33] the cell line and cell density,[34] composition of particles,[35] surface properties (surface hydrophobicity/hydrophilicity and surface charges),[34,35] temperature, and so on. In the present instance, since NP2K, NP3K, and NP4K nanoparticles had main differences in their average size as well as the length of PCL segments in mPEG-PCLs, it may be drawn that the smaller NP2K nanoparticles had shorter PCL segments and more hydrophilic
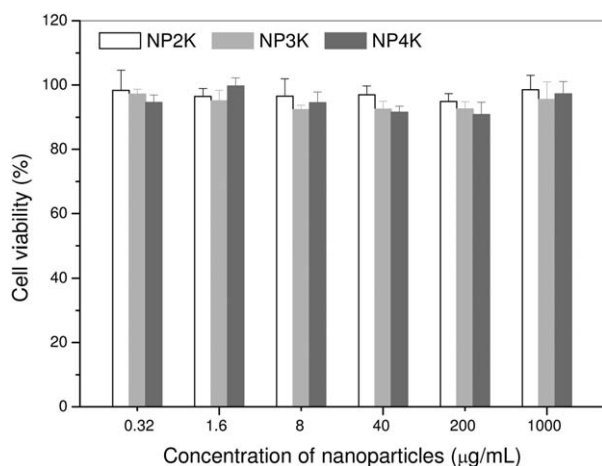

Figure 3. Viability of Hela cells respectively cultured *in vitro* with NP2K (A), NP3K (B), and NP4K (C) nanoparticles for 48 h.
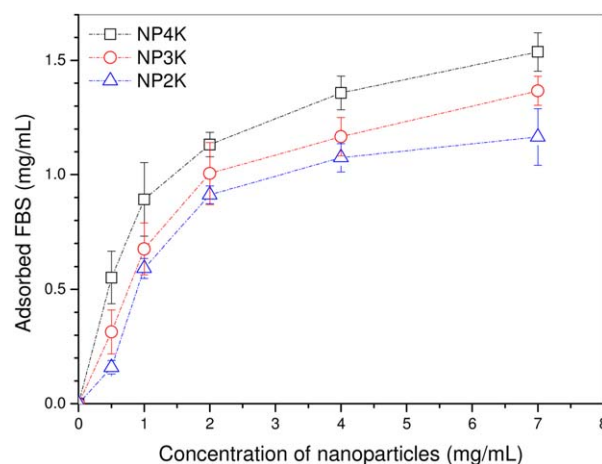

Figure 4. FBS adsorption of different nanoparticles (FBS concentration: 20%, culture conditions: 37°C, 2 h). [Color figure can be viewed in the online issue, which is available at wileyonlinelibrary.com.]
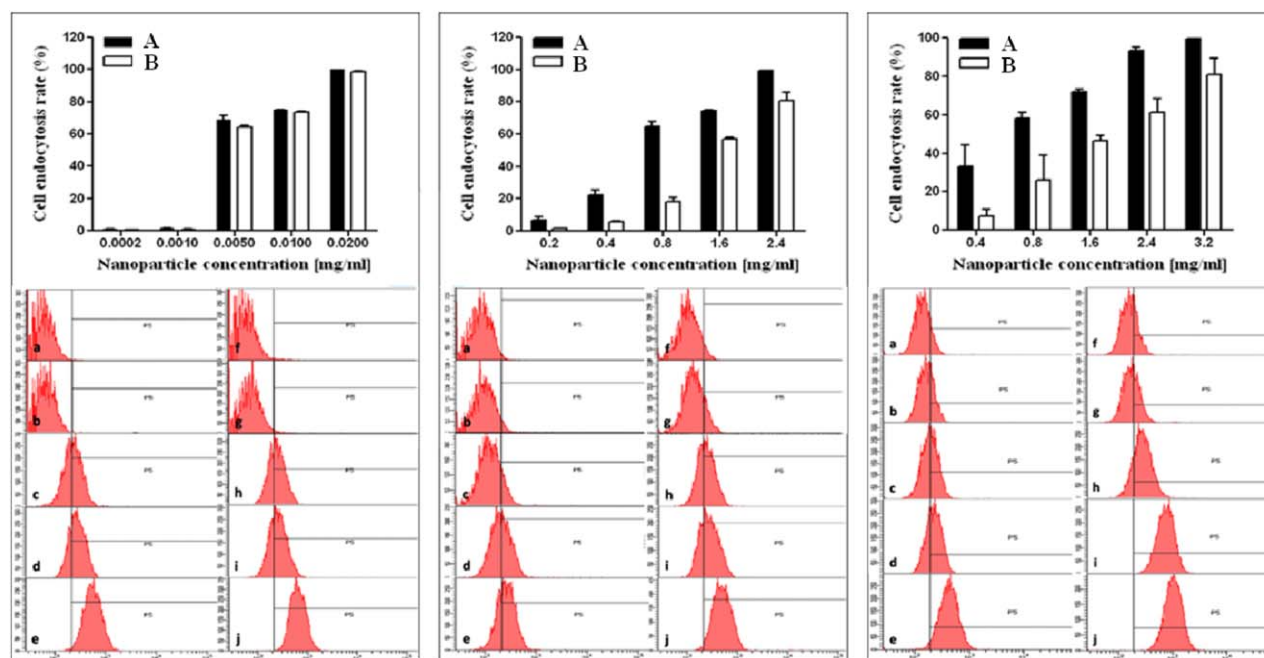
Figure 5. Hela cell endocytosis rate of nanoparticles at various nanoparticle concentrations (culture time: 37°C, 60 min). Left column: NP2K (left panels: a–e (0.0002–0.0200 mg/mL), in FBS-free medium, A; right panels: f–j (0.0002–0.0200 mg/mL), in FBS-contained medium, B); middle column: NP3K (left panels: a–e (0.2–2.4 mg/mL), in FBS-free medium, A; right panels: f–j (0.2–2.4 mg/mL), in FBS-contained medium, B); and right column NP4K (left panels: a–e (0.4–3.2 mg/mL), in FBS-free medium, A; right panels: f–j (0.4–3.2 mg/mL), in FBS-contained medium, B). [Color figure can be viewed in the online issue, which is available at wileyonlinelibrary.com.]

surface, which would result in lower FBS-adsorption (see Figure 4), and in turn, higher endocytosis rate. On the other hand, the larger NP4K nanoparticles had longer PCL segments and less hydrophilic surface, leading to higher FBS-adsorption (see Figure 4), and thus, lower endocytosis rate.

To see the effect of culture-time of FBS-adsorbed nanoparticles on the cell uptake, NP2K, NP3K, and NP4K nanoparticles were respectively incubated with Hela cells at a fixed nanoparticle concentration of 0.2 mg/mL in the media without or with 10% FSB for various periods of time changing from 5 to 180 min, and their endocytosis rate as well as fluorescent images were analyzed. Figure 6 presents some representative fluorescent images for three types of Hela cells cultured with nanoparticles for a same period of time (60 min). These images approximately show that in the cases of FBS-free medium (left column), RhB fluorescent intensity showed that more NP2K nanoparticles were taken by Hela cells than two other types of

nanoparticles; and in the cases of FBS-contained medium (right column), a decreasing trend in fluorescent intensity was recorded for NP2K, NP3K, and NP4K nanoparticles. In addition, fluorescent intensity for NP3K and NP4K nanoparticles cultured in the FBS-contained medium was much lower than in the FBS-free medium. These results were in rough agreement with that illustrated in Figure 5.

Figure 7 shows endocytosis rates for three types of nanoparticles cultured with Hela cells at a particle concentration of 0.2 mg/mL over various periods of time up to 180 min. As mentioned earlier in Figure 5, to reach an approximately similar endocytosis level, the needed particle concentration for NP2K nanoparticles was much lower in comparison to NP3K or NP4K nanoparticles. In order to compare the endocytosis rate on the same baseline for three types of nanoparticles, a particle concentration of 0.2 mg/mL was selected at a compromising level in the present instance, which is much higher than the necessary one for NP2K nanoparticles but quite low for NP3K and NP4K nanoparticles (see Figure 5). It can be observed from Figure 7 that in the case of NP2K nanoparticles, their endocytosis rate reached more than 90% after 5-min culture, and after that, it seemed not to change significantly; and in addition, the FBS-free or FBS-contained medium did not impose significantly impacts on the endocytosis rate of NP2K nanoparticles. The Hela cell uptake behavior matching with NP2K nanoparticles could be ascribed to the too high particle concentration used, and thus, the internalization of NP2K associated with Hela cells could be very fast and saturated in a short period of time, for example, 5 min, as indicated in Figure 7 by the high endocytosis rate.

Table II. EC_{50} (mg/mL) for Three Types of Nanoparticles Cultured with Hela Cells[a]

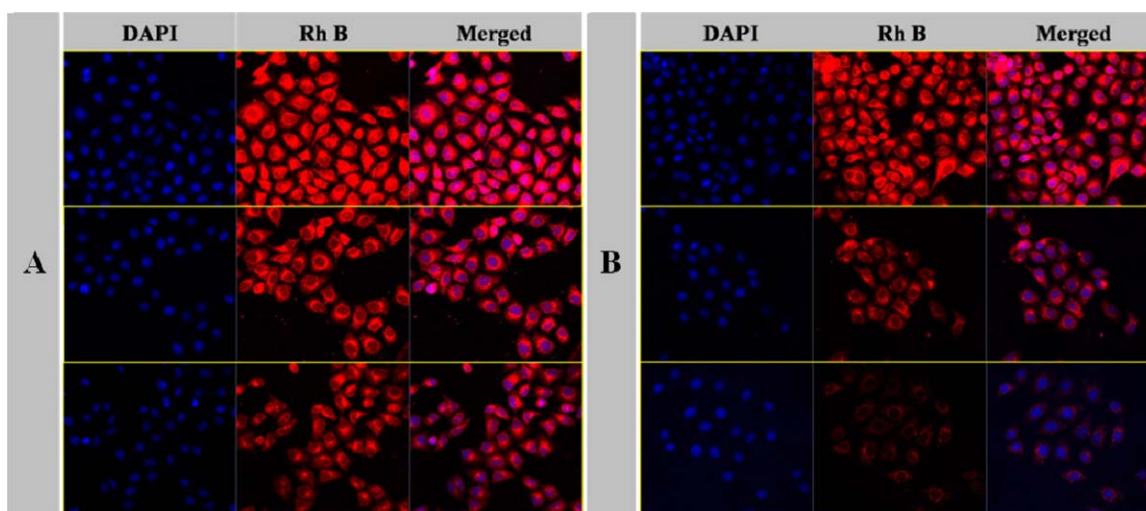| Sample name	EC_{50} in FBS-free medium (A)	EC_{50} in FBS-contained medium (B)	ΔEC_{50} (B–A)
NP2K	0.006	0.007	0.001
NP3K	0.633	1.459	0.796
NP4K	0.670	1.762	1.092

[a] Culture time: 60 min.

Figure 6. Fluorescent images of Hela cells cultured with NP2K (upper line), NP3K (middle line), and NP4K (lower line) nanoparticles for 60 min (concentration of nanoparticles: 0.2 mg/mL; DAPI staining (blue); RhB fluorescence (red); left column (A): in FBS-free medium; right column (B): in FBS-contained medium (10% FBS). [Color figure can be viewed in the online issue, which is available at wileyonlinelibrary.com.]

With respective to NP3K and NP4K nanoparticles, they both showed uptrends with small differences in the increment rates for their endocytosis rate as the culture time was extended. When cultured at a particle concentration of 0.2 mg/mL in the FBS-contained medium, these two types of nanoparticles seemed to be completely obstructed from being internalized even if they were cultured with Hela cells for 180 min (see middle and right columns in Figure 7). Under this circumstance, FBS-adsorption should be considered as a key factor that can regulate the uptake behavior of NP3K and NP4K nanoparticles. FBS is known to be a type of "bystander" protein, namely, a protein for which no specific cellular recognition mechanism exists.[36] Thus, the adsorbed FBS proteins onto the surface of NP3K and NP4K nanoparticles in fact act as a protective layer, shielding the surface of
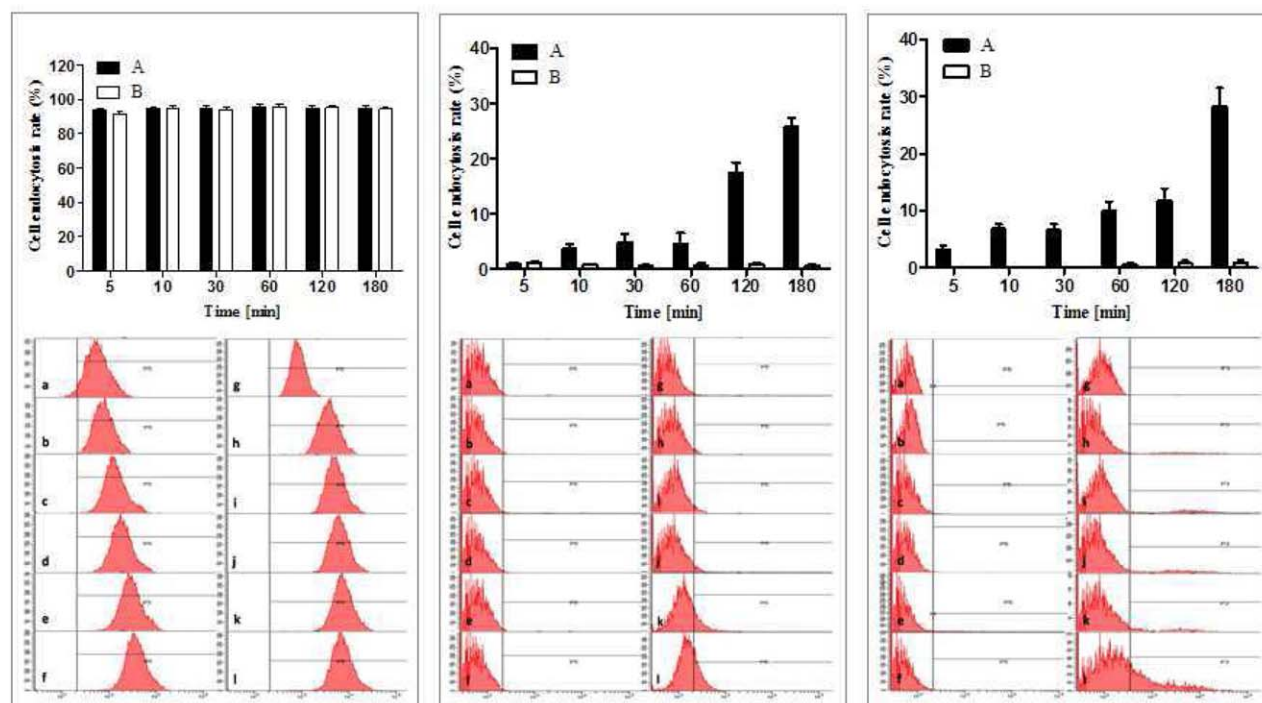

Figure 7. Hela cell endocytosis rate of nanoparticles as function of incubation time (nanoparticle concentration: 0.2 mg/mL). Left column: NP2K (left panels: a–f (5–180 min), in FBS-free medium, A; right panels: g–l (5–180 min), in FBS-contained medium, B); middle column: NP3K (left panels: a–f (5–180 min), in FBS-free medium, A; right panels: g–l (5–180 min), in FBS-contained medium, B); and right column NP4K (left panels: a–f (5–180 min), in FBS-free medium, A; right panels: g–l (5–180 min), in FBS-contained medium, B). [Color figure can be viewed in the online issue, which is available at wileyonlinelibrary.com.]
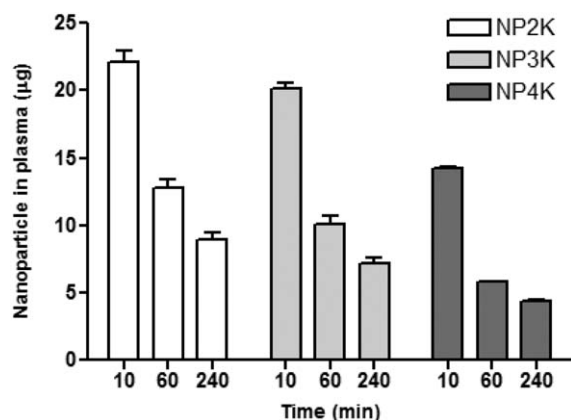
Figure 8. Nanoparticle content in mouse plasma after injection with an equivalent amount of nanoparticles for various periods of time (dose: 50 mg/kg).

the nanoparticles from interactions with the cells, resulting in much lower internalization of nanoparticles when they were cultured in the FBS-contained medium than in the FBS-free medium.

Blood Clearance

The circulation duration of drug-carried nanoparticles in the blood is a key factor for assessing their capability of drug-delivery. In principle, *in vivo* clearance of nanoparticles involves three main pathways: (a) disintegration of nanoparticles due to protein adsorption and zymohydrolysis, (b) heterologous removal opsonized by immune cells, and (c) filtration by organs with fenestrated vasculature. It is generally accepted that the physicochemical properties of nanoparticles, mainly including surface charge, hydrophobicity, particle size, surface curvature, and surface area, can significantly influence protein adsorption to the surface of nanoparticles. Hydrophobicity of the nanoparticle surface is one of main factors that are related to the protein adsorption in plasma. In general, higher hydrophobicity of nanoparticle surface could incur greater and faster protein binding.[37–39] As mentioned earlier, besides the significant differences in particle sizes (see Table I), NP2K, NP3K, and NP4K nanoparticles could also have differences in their hydrophobicity because of different molar ratios of mPEG to PCL (see Table I). To see whether the different nanoparticles would have differences in their clearance from blood, blood samples obtained from mice that were intravenously injected with an equal amount of nanoparticles were qualitatively examined using fluorescent analysis, and the calculated particle content in the mouse plasma was depicted in Figure 8. It can be noted that nanoparticle content in the plasma gradually decreased over the extended time and there were significant differences ($P<0.05$) in their decreasing rates. At each measurement point, nanoparticle content in the plasma was ranged in a decreasing order of NP2K, NP3K, and NP4K with significant differences ($P<0.05$). Considering the differences in the average particle size and surface hydrophilicity of these nanoparticles, these results suggest that nanoparticles with smaller size and relatively hydrophilic surface, namely, NP2K nanoparticles in the present instance, are able to circulate in blood for a relatively long duration.

CONCLUSIONS

Several types of nanoparticles were successfully produced using different RhB-labeled mPEG-PCL copolymers with various molar ratios of mPEG to PCL. It was found that smaller mPEG-PCL nanoparticles with a higher mPEG/PCL molar ratio showed a less ability to adsorb FBS and can be easily internalized by Hela cells at lower particle doses in both FBS-free and FBS-contained media in comparison to the larger mPEG-PCL nanoparticles with relatively low mPEG/PCL molar ratios. When the larger mPEG-PCL nanoparticles with relatively low mPEG/PCL molar ratios were exposed to FBS-free or FBS-contained media at different doses or various culture times, the FBS-contained medium could significantly obstruct their internalization by Hela cells. The blood clearance testing confirmed that the smaller mPEG-PCL nanoparticles with a higher mPEG/PCL molar ratio will have potential to circulate in blood for a relatively long duration than those larger mPEG-PCL nanoparticles with relatively low mPEG/PCL molar ratios. These results suggest that FBS, a common protein, is able to significantly regulate the cell uptake of these mPEG/PCL nanoparticles *in vitro*, and on the other hand, the size and mPEG/PCL molar ratio of mPEG/PCL nanoparticles are closely correlated to their blood clearance.

REFERENCES

1. Cuong, N. V.; Hsieh, M. F.; Chen, Y. T.; Liau, I. *J. Appl. Polym. Sci.* **2010**, *117*, 3694.

2. Zhang, L.; Fu, J. Y.; Xia, Z. X.; Wu, P.; Zhang, X. F. *J. Appl. Polym. Sci.* **2011**, *122*, 758.

3. Zhang, H. Y.; Lu., X. *Asian Pac. J. Cancer Prev.* **2015**, *16*, 4045.

4. Gao, S. R.; Li, L. M.; Xia, H. P.; Wang, G. M.; Xu, H. Y.; Wang, A. R. *Asian Pac. J. Cancer Prev.* **2015**, *16*, 4037.

5. Hossain, M. K.; Cho, H. Y.; Kim, K. J.; Choi, J. W. *Biosens. Bioelectron.* **2015**, *71*, 300.

6. Abbasi, A. Z.; Prasad, P.; Cai, P.; He, C.; Foltz, W. D.; Amini, M. A.; Gordijo, C. R.; Rauth, A. M.; Wu, X. Y. *J. Control. Release* **2015**, *209*, 186.

7. Gou, M.; Wei, X.; Men, K.; Wang, B.; Luo, F.; Zhao, X.; Wei, Y.; Qian, Z. *Curr. Drug Targets* **2011**, *12*, 1131.

8. Gou, M.; Men, K.; Shi, H.; Xiang, M.; Zhang, J.; Song, J.; Long, J.; Wan, Y.; Luo, F.; Zhao, X.; Qian, Z. *Nanoscale* **2011**, *3*, 1558.

9. Wei, X.; Gong, C.; Gou, M.; Fu, S.; Guo, Q.; Shi, S.; Luo, F.; Guo, G.; Qiu, L.; Qian, Z. *Int. J. Pharm.* **2009**, *381*, 1.

10. Gou, M.; Zheng, X.; Men, K.; Zhang, J.; Wang, B.; Lv, L.; Wang, X.; Zhao, Y.; Luo, F.; Chen, L.; Zhao, X.; Wei, Y.; Qian, Z. *Pharm. Res.* **2009**, *26*, 2164.

11. Lynch, I.; Dawson, K. A. *Nano Today* **2008**, *3*, 40.

12. Nel, A. E.; Maedler, L.; Velegol, D.; Xia, T.; Hoek, E. M. V.; Somasundaran, P.; Klaessig, F.; Castranova, V.; Thompson, M. *Nat. Mater.* **2009**, *8*, 543.

13. Zhu, Y.; Li, W.; Li, Q.; Li, Y.; Li, Y.; Zhang, X.; Huang, Q. *Carbon* **2009**, *47*, 1351.

14. Patel, P. C.; Giljohann, D. A.; Daniel, W. L.; Zheng, D.; Prigodich, A. E.; Mirkin, C. A. *Bioconjugate Chem.* **2010**, *21*, 2250.

15. Bajaj, A.; Samanta, B.; Yan, H.; Jerry, D. J.; Rotello, V. M. *J. Mater. Chem.* **2009**, *19*, 6328.

16. Stayton, I.; Winiarz, J.; Shannon, K.; Ma, Y. *Anal. Bioanal. Chem.* **2009**, *394*, 1595.

17. Guarnieri, D.; Guaccio, A.; Fusco, S.; Netti, P. A. *J. Nanopart. Res.* **2011**, *13*, 4295.

18. Ehrenberg, M. S.; Friedman, A. E.; Finkelstein, J. N.; Oberdoerster, G.; McGrath, J. L. *Biomaterials* **2009**, *30*, 603.

19. Jiang, X.; Weise, S.; Hafner, M.; Roecker, C.; Zhang, F.; Parak, W. J.; Nienhaus, G. U. *J. Roy. Soc. Interface* **2010**, *7*, S5.

20. Iversen, T. G.; Skotland, T.; Sandvig, K. *Nano Today* **2011**, *6*, 176.

21. Dos Santos, T.; Varela, J.; Lynch, I.; Salvati, A.; Dawson, K. A. *Plos One* **2011**, *6*, e24438.

22. Ge, C.; Du, J.; Zhao, L.; Wang, L.; Liu, Y.; Li, D.; Yang, Y.; Zhou, R.; Zhao, Y.; Chai, Z.; Chen, C. *Proc. Natl. Acad. Sci. USA* **2011**, *108*, 16968.

23. Hu, W.; Peng, C.; Lv, M.; Li, X.; Zhang, Y.; Chen, N.; Fan, C.; Huang, Q. *ACS Nano* **2011**, *5*, 3693.

24. Shi, J.; Karlsson, H. L.; Johansson, K.; Gogvadze, V.; Xiao, L.; Li, J.; Burks, T.; Garcia-Bennett, A.; Uheida, A.; Muhammed, M.; Mathur, S.; Morgenstern, R.; Kagan, V. E.; Fadeel, B. *ACS Nano* **2012**, *6*, 1925.

25. Haniu, H.; Saito, N.; Matsuda, Y.; Kim, Y. A.; Park, K. C.; Tsukahara, T.; Usui, Y.; Aoki, K.; Shimizu, M.; Ogihara, N.; Hara, K.; Takanashi, S.; Okamoto, M.; Ishigaki, N.; Nakamura, K.; Kato, H. *Int. J. Nanomed.* **2011**, *6*, 3295.

26. Dutta, D.; Sundaram, S. K.; Teeguarden, J. G.; Riley, B. J.; Fifield, L. S.; Jacobs, J. M.; Addleman, S. R.; Kaysen, G. A.; Moudgil, B. M.; Weber, T. *J. Toxicol. Sci.* **2007**, *100*, 303.

27. Buijs, J.; Vera, C. C.; Ayala, E.; Steensma, E.; Hakansson, P.; Oscarsson, S. *Anal. Chem.* **1999**, *71*, 3219.

28. Gong, C.; Qian, Z.; Liu, C.; Huang, M.; Gu, Y.; Wen, Y.; Kan, B.; Wang, K.; Dai, M.; Li, X.; Gou, M.; Tu, M.; Wei, Y. *Smart Mater. Struct.* **2007**, *16*, 927.

29. Li, X.; Zhang, Z.; Li, J.; Sun, S.; Weng, Y.; Chen, H. *Nanoscale* **2012**, *4*, 4667.

30. Kim, B. S.; Oh, J. M.; Kim, K. S.; Seo, K. S.; Cho, J. S.; Khang, G.; Lee, H. B.; Park, K.; Kim, M. S. *Biomaterials* **2009**, *30*, 902.

31. Diezi, T. A.; Bae, Y.; Kwon, G. S. *Mol. Pharm.* **2010**, *7*, 1355.

32. Luo, Q. L.; Andrade, J. D. *J. Colloid. Interf. Sci.* **1998**, *200*, 104.

33. Zauner, W.; Farrow, N. A.; Haines, A. M. R. *J. Control. Release* **2001**, *71*, 39.

34. Jung, T.; Kamm, W.; Breitenbach, A.; Kaiserling, E.; Xiao, J. X.; Kissel, T. *Eur. J. Pharm. Biopharm.* **2000**, *50*, 147.

35. Foster, K. A.; Yazdanian, M.; Audus, K. L. *J. Pharm. Pharmacol.* **2001**, *53*, 57.

36. Walczyk, D.; Bombelli, F. B.; Monopoli, M. P.; Lynch, I.; Dawson, K. A. *J. Am. Chem. Soc.* **2010**, *132*, 5761.

37. Yadav, K. S.; Jacob, S.; Sachdeva, G.; Chuttani, K.; Mishra, A. K.; Sawant, K. K. *J. Microencapsul.* **2011**, *28*, 729.

38. Vij, N.; Min, T.; Marasigan, R.; Belcher, C. N.; Mazur, S.; Ding, H.; Yong, K. T.; Roy, I. *J. Nanobiotec.* **2010**, *8*, 22.

39. Ratzinger, G.; Laenger, U.; Neutsch, L.; Pittner, F.; Wirth, M.; Gabor, F. *Langmuir* **2010**, *26*, 1855.